# Screening of 4*f* moments and delocalization in the compressed light rare earths

A. K. McMahan,[1] R. T. Scalettar,[2] and M. Jarrell[3]
[1]*Physical and Life Sciences Directorate, Lawrence Livermore National Laboratory, Livermore, California 94550, USA*
[2]*Physics Department, University of California, Davis, California 95616, USA*
[3]*Department of Physics and Astronomy, Louisiana State University, Baton Rouge, Louisiana 70803, USA*
(Received 24 August 2009; revised manuscript received 29 October 2009; published 2 December 2009)

Spin and charge susceptibilities and the $4f^n$, $4f^{n-1}$, and $4f^{n+1}$ configuration weights are calculated for compressed Ce ($n=1$), Pr ($n=2$), and Nd ($n=3$) metals at 632 K using dynamical mean-field theory combined with the local-density approximation. At ambient and larger volumes these trivalent rare earths are pinned at sharp $4f^n$ configurations, their 4*f* moments assume atomic-limiting values, are unscreened, and the 4*f* charge fluctuations are small indicating little *f* state density near the Fermi level. Under compression there is dramatic screening of the moments and an associated increase in both the 4*f* charge fluctuations and static charge susceptibility. These changes coincide with growing weights of the $4f^{n-1}$ configurations, which it is argued are better measures of delocalization than the $4f^{n+1}$ weights which are compromised by an increase in the number of 4*f* electrons caused by rising 6*s* and 6*p* bands. This process is continuous and prolonged as a function of volume, with striking similarity among the three rare earths, aside from the effects moderating and shifting to smaller volumes for the heavier members. While the present calculations have been carried out at 632 K for reasons of computational expense, tests of the temperature sensitivities are used to indicate the kind of modest changes expected at room temperature

DOI: 10.1103/PhysRevB.80.235105 PACS number(s): 71.27.+a, 71.20.Eh, 75.20.Hr

## I. INTRODUCTION

The trivalent rare-earth series is an important but not well understood test ground for the study of strong electron correlation and the manner in which its effects diminish as the 4*f* electrons delocalize under pressure. These metals appear initially to remain localized as they pass through a sequence of high-symmetry close-packed phases keyed to 3*d*-band occupancy[1] and then on further compression, eventually reach low-symmetry early actinidelike structures suggestive of *f*-electron bonding.[2–4] Transitions in the region between these two limits may exhibit unusually large-volume changes. While not the case for Nd,[5,6] the $\gamma$-$\alpha$ "volume collapse" of 15% in Ce is well known[7–10] and similar collapses occur in Pr (9%),[11–15] Gd (5%),[16] and Dy (6%).[17] Magnetic properties at atmospheric pressure are generally consistent with atomic 4*f* Hund's rules moments[4,18] while the susceptibility for the collapsed $\alpha$-Ce phase[7] and for early actinide analogs[19] is temperature-independent, enhanced Pauli paramagnetic, indicating absent or screened moments. On the other hand, high-energy neutron-scattering measurements for Ce (Ref. 20) and x-ray emission spectroscopy for Gd (Ref. 21) continue to detect 4*f* moments in the collapsed phases, possibly sensing underlying "bare" moments in spite of screening effects. The 4*f* electron delocalization itself may be examined using resonant inelastic x-ray scattering determination of the probabilities of finding $f^{n\pm1}$ configurations in a compressed rare earth of nominal $f^n$ character.[21,22]

There are at present two viable explanations for the Ce collapse, with possible implications for the other trivalent rare earths. One is that it is driven by a Mott transition (MT) in the 4*f* electrons[23,24] while the other Kondo volume collapse (KVC) model points to rapid volume-dependent changes in screening of the 4*f* moments by the valence electrons.[25–28] The conflict between these scenarios is exaggerated by the use of incompatible approximations. Polarized local-density approximation (LDA), LDA+*U*, and self-interaction corrected LDA calculations have been used to support the MT picture.[29–35] While valuable, these are still *static* mean-field treatments which yield either completely itinerant (no 4*f* Hubbard structure) or completely localized (Hubbard splitting but no Fermi-level 4*f* structure) solutions, thus indicating a too abrupt picture of the collapse transitions. On the other hand, the Anderson impurity model treatments[25–28] used to elucidate the KVC scenario can be faulted for omitting direct *f*-*f* hybridization and Kondo lattice effects, and one may worry whether $O(1/N)$ solutions[36] might favor the localized limit.

The combination (LDA+DMFT) (Refs. 37 and 38) of LDA input with truly correlated dynamical mean-field theory (DMFT) (Refs. 39 and 40) solutions has offered a new perspective which has generally been supportive of the KVC scenario for Ce.[41–46] Such calculations for Ce also point to ongoing 4*f* delocalization in the relevant volume range, a critical driver of Mott transitions.[42,43] To further clarify the behavior of the compressed trivalent rare earths, the present paper reports LDA+DMFT calculations of the 4*f* spin and charge susceptibilities and the $4f^n$, $4f^{n\pm1}$ configuration weights at 632 K for the first three members, Ce ($n=1$), Pr ($n=2$), and Nd ($n=3$). This work follows an earlier effort which examined the equation of state and spectra for the same materials.[44] Here we confirm that Ce, Pr, and Nd remain localized at pressures up through the face-centered-cubic (fcc, $\gamma$ for Ce) phases as indicated by sharp $4f^n$ populations, unscreened moments with atomic-limiting values, and small charge fluctuations indicating little 4*f* state density overlapping the Fermi level. On subsequent compression there is rapid and dramatic screening of the moments and concurrent increase in charge fluctuations and the static charge susceptibility. These changes also coincide with rapid growth in the $4f^{n-1}$ configuration weights, which we argue

 

offer a truer measure of delocalization than do the $4f^{n+1}$ weights which are complicated by the overall increase in the number of $4f$ electrons due to rising $6s$ and $6p$ bands. These trends are continuous and prolonged as a function of compression and strikingly similar among the three rare earths, suggesting a robust underlying progression which must first be acknowledged before tackling in general the location or absence of volume collapse transitions at various stages along the course of this evolution.

Two caveats should be made about the present work. First it is motivated by and intended to address volume-dependent changes encountered in isothermal diamond-anvil cell experiments which are primarily carried out at room temperature, although occasionally above. Thus, for example, differences between Hubbard and periodic Anderson models which may be exposed at very low temperatures are beyond the scope of the present work.[47–49] Secondly, due to a $\sim 1/T^3$ computational cost, we have been practically limited to a lowest temperature of 632 K (4 mRy). Nonetheless, tests of the temperature sensitivities suggest that the primary change on reducing the temperature to 300 K is to shift to somewhat larger volumes the onset with compression of the dramatic screening and delocalization effects documented here at 632 K.

In the remainder of this paper, the susceptibility and configuration weight formalisms are first reviewed in Secs. II and III, respectively. Computational details are given in Sec. IV, results in Sec. V, and a summary in Sec. VI. The Appendix discusses the optimal disposition of diagonal, one-body $f$-$f$ terms used here in the quantum Monte Carlo (QMC) solution of auxiliary impurity problem.

## II. SUSCEPTIBILITY

The important local $4f$ susceptibilities for real, multiband systems would appear to be associated with the total spin $\mathbf{S}$, orbital angular momentum $\mathbf{L}$, total angular momentum $\mathbf{J}=\mathbf{L}+\mathbf{S}$, and charge

$$\chi_S(\tau) = \langle T_\tau \hat{\mathbf{S}}(\tau) \cdot \hat{\mathbf{S}}(0) \rangle, \tag{1}$$

$$\chi_L(\tau) = \langle T_\tau \hat{\mathbf{L}}(\tau) \cdot \hat{\mathbf{L}}(0) \rangle, \tag{2}$$

$$\chi_J(\tau) = \langle T_\tau \hat{\mathbf{J}}(\tau) \cdot \hat{\mathbf{J}}(0) \rangle, \tag{3}$$

$$\chi_c(\tau) = \langle T_\tau [\hat{n}_f(\tau) - n_f][\hat{n}_f(0) - n_f] \rangle \tag{4}$$

for electrons in the $4f$ shell on a particular site and with $T_\tau$ the imaginary time $\tau$ ordering operator. In the last, $\hat{n}_f$ is the total number operator $\Sigma_{m,\sigma} \hat{n}_{m\sigma}$ with $m=-3,-2,\ldots,3$ and $n_f$ is its generally nonintegral expectation. For cubic symmetry,

$$\chi_S(\tau) = 3\langle T_\tau \hat{S}_z(\tau)\hat{S}_z(0)\rangle = \frac{3}{4} \sum_{m,\sigma,m',\sigma'} \sigma\sigma' \langle T_\tau \hat{n}_{m\sigma}(\tau)\hat{n}_{m'\sigma'}(0)\rangle$$

$$= \frac{3}{4}\langle T_\tau [\hat{n}_\uparrow(\tau) - \hat{n}_\downarrow(\tau)][\hat{n}_\uparrow(0) - \hat{n}_\downarrow(0)]\rangle, \tag{5}$$

where $\hat{n}_\sigma \equiv \Sigma_m \hat{n}_{m\sigma}$ is the total number operator for a given spin $\sigma \equiv 2m_s = \pm 1$ summed over orbitals $m \equiv m_f$. Aside from the factor of 3/4 this is the spin susceptibility of the two-band model of Koga *et al.*[50] or for $\tau=0$, the same factor times the bare local moment $m_z^2$ of one-band Hubbard and Anderson models. Similarly $\chi_L(\tau) = 3\langle T_\tau \hat{L}_z(\tau)\hat{L}_z(0)\rangle$ for cubic symmetry and thus

$$\chi_L(\tau) = 3 \sum_{m,\sigma,m',\sigma'} mm' \langle T_\tau \hat{n}_{m\sigma}(\tau)\hat{n}_{m'\sigma'}(0)\rangle, \tag{6}$$

which is 3/4 times the orbital susceptibility of the two-band model of Koga *et al.*,[50] taking the orbital angular momentum $l=1/2$ ($m=-1/2,1/2$) instead of the present $l=3$.

### A. Spin susceptibility $\chi_J(\tau)$

In the presence of the spin-orbit interaction, it may be more useful to work in a relativistic basis $j=l\pm 1/2 = 5/2, 7/2$ with magnetic quantum numbers $\nu=-j,-j+1,\ldots,j$. Again for cubic symmetry,

$$\chi_J(\tau) = 3 \sum_{j,\nu,j',\nu'} \nu\nu' \langle T_\tau \hat{n}_{j\nu}(\tau)\hat{n}_{j'\nu'}(0)\rangle. \tag{7}$$

For DMFT calculations which include spin orbit and the Hubbard repulsion $U$ but omit the Hund's rule intraatomic exchange terms, a reasonable approximation to the self-energy is $\Sigma_{j,\nu,j',\nu'}(i\omega) \sim \delta_{j,j'}\delta_{\nu,\nu'}\Sigma_j(i\omega)$, which approximates the cubic environment of the auxiliary impurity problem by a spherical one. A consistent approximation to $\langle T_\tau \hat{n}_{j\nu}(\tau)\hat{n}_{j'\nu'}(0)\rangle$ is

$$\langle T_\tau \hat{n}_{j\nu}(\tau)\hat{n}_{j'\nu'}(0)\rangle \sim \begin{cases} N_j(\tau)/(2j+1) & \text{if } j=j',\ \nu=\nu' \\ D_{jj}(\tau)/[j(2j+1)] & \text{if } j=j',\ \nu\neq\nu' \\ D_{jj'}(\tau)/[(2j+1)(2j'+1)] & \text{if } j\neq j' \end{cases}, \tag{8}$$

where

$$N_j(\tau) \equiv \sum_\nu \langle T_\tau \hat{n}_{j\nu}(\tau)\hat{n}_{j\nu}(0)\rangle, \tag{9}$$

$$D_{jj}(\tau) \equiv \frac{1}{2} \sum_{\nu\nu'}^{\nu\neq\nu'} \langle T_\tau \hat{n}_{j\nu}(\tau)\hat{n}_{j\nu'}(0)\rangle,$$

$$D_{j\neq j'}(\tau) \equiv \frac{1}{2}\sum_{\nu\nu'} \langle T_\tau [\hat{n}_{j\nu}(\tau)\hat{n}_{j'\nu'}(0) + \hat{n}_{j'\nu'}(\tau)\hat{n}_{j\nu}(0)]\rangle \tag{10}$$

with $\nu$ ranging over the $2j+1$ states of $j$ (similarly $\nu'$ and $j'$). Then

$$\chi_J(\tau) = \sum_j (j+1)[jN_j(\tau) - D_{jj}(\tau)]. \tag{11}$$

Note that at $\tau=0$, $N_j(0)=n_j$, and $D_{jj'}(0)=d_{jj'}$ where the number of electrons in the $4f$ shell is $n_f=n_{5/2}+n_{7/2}$ and the associated double occupation is $d_f=d_{5/2,5/2}+d_{5/2,7/2}+d_{7/2,7/2}$.

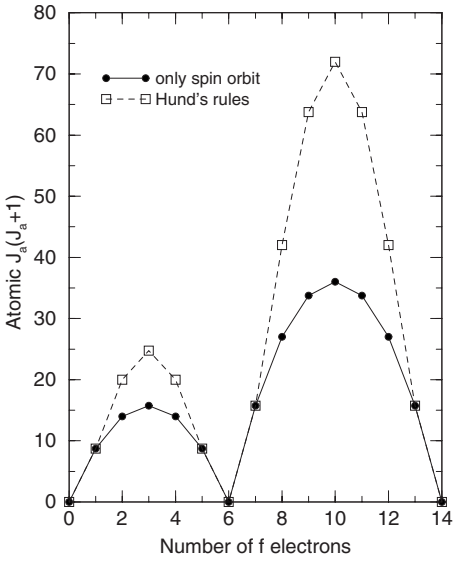


FIG. 1. Atomic moments $\langle \hat{\mathbf{J}}^2 \rangle = J_a(J_a+1)$ for the rare earths.

The *bare* or instantaneous local moments corresponding to each of Eqs. (1)–(3) are given by their $\tau=0$ values, e.g.,

$$J_b(J_b+1) = \langle \hat{\mathbf{J}}^2 \rangle = \chi_J(\tau=0) = \sum_j (j+1)[jn_j - d_{jj}]. \tag{12}$$

For $f$ electrons with integer $n_f=n$ shell populations $0 \le n \le 14$, one might expect in the strongly localized, atomic limit that

$$n_{5/2} = \min(n,6),$$

$$d_{5/2,5/2} = n_{5/2}(n_{5/2}-1)/2,$$

$$n_{7/2} = \max(0,n-6),$$

$$d_{7/2,7/2} = n_{7/2}(n_{7/2}-1)/2,$$

which leads to the filled data points (only spin orbit) in Fig. 1. Inclusion of the appropriate intra-atomic exchange terms would give the correct Hund's rules values designated by the open squares. For the case of Ce, such terms correspond to an exchange interaction $J$ of about 0.7 eV,[51] as compared to a spin-orbit splitting of about 0.4 eV.[52] Unfortunately it is still a challenge to treat the full rotationally invariant set of Hund's rules exchange terms in DMFT calculations. The spin-orbit-only results are seen to give the correct qualitative behavior with filling and the correct values of $\langle \hat{\mathbf{J}}^2 \rangle$ for subshells with one or no holes or electrons. As will be seen in this paper, they also appear to give the qualitatively correct evolution from localized to itinerant behavior with compression since much of that originates from volume-dependent changes in the double occupation which is captured correctly.

Information about *screened* moments comes from the static susceptibility $\chi_J(\omega=0)$. Given Curie-Weiss behavior, an effective moment can be extracted from the slope of $\chi_J(\omega=0)$ versus $T^{-1}$, thus

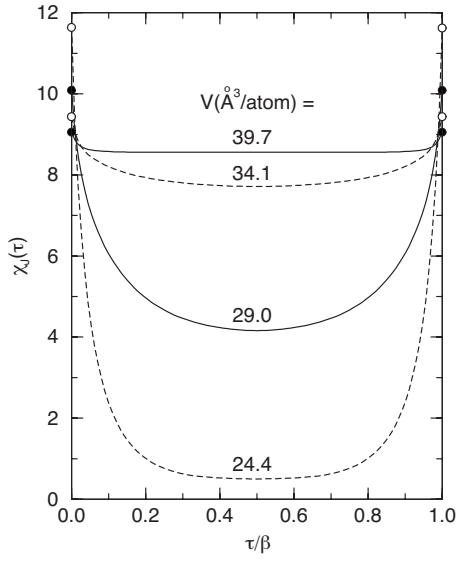


FIG. 2. $\chi_J(\tau)$ for Ce at 632 K and various volumes. The $\tau=0$ values (circles) give the bare moment squared $\langle \hat{\mathbf{J}}^2 \rangle = J_b(J_b+1)$ while the $\tau$ average gives the screened quantity $J_s(J_s+1)$. There is little screening at large volume while the two moments are quite different at small volume. The $\alpha$ and $\gamma$ sides of the collapse are at volumes of 27.8 and 33.1 Å$^3$/atom, respectively, correspondingly roughly to the middle two curves. The equilibrium volume is 34.4 Å$^3$/atom.

$$J_s(J_s+1) = T\chi_J(\omega=0) = \frac{1}{\beta}\int_0^\beta d\tau \chi_J(\tau). \tag{13}$$

At small volume (strong hybridization) and low temperature, $\chi_J(\tau)$ falls away between its maximal values at $\tau=0$ and $\beta$ as seen in Fig. 2, which leads to $J_s < J_b$. On the other hand, at large volume and thus weak hybridization, $\hat{\mathbf{J}}$ approximately commutes with the Hamiltonian so that $\chi_J(\tau) \sim$ constant and thus there is no screening ($J_s \sim J_b$). There is also no screening in the high-temperature limit since $\chi_J(\tau) \to \chi_J(0)$ as $0 \le \tau \le 1/T \to 0$, although such moments become significantly larger than those at low temperature for the present materials because of high temperature increases in $n_f$. Note that Eq. (12) becomes $J_b(J_b+1) = 12.75 n_f(1-n_f/14)$ for uncorrelated, equally populated $f$ states where $\langle \hat{n}_{j\nu}\hat{n}_{j'\nu'} \rangle \sim (n_f/14)^2$ for $j\nu \neq j'\nu'$.

The present calculations have been carried out at 632 K due to a $1/T^3$ computational expense which has precluded examination of room temperature. Nonetheless, one can probe the relevant temperature sensitivities by raising the temperature instead and Fig. 3(a) compares $J_s(J_s+1)$ for Ce at 948 K (6 mRy) and 632 K (4 mRy) as obtained with $L=80$ time slices. Since raising the temperature decreases screening, the 948 K result lies above the 632 K curve except at large volume where both moments are unscreened and equal to the atomic value. The predominant visual difference is that the lower temperature curve appears shifted to larger volume by $\sim 2$ Å$^3$/atom at half the atomic value. The volume offset between where the Kondo temperature $T_K$ equals 948 versus 632 K is 0.9 Å$^3$/atom,[25] by comparison, which should be smaller since $J_s(J_s+1)/J_b(J_b+1) = 0.5$ at $T_K$ and

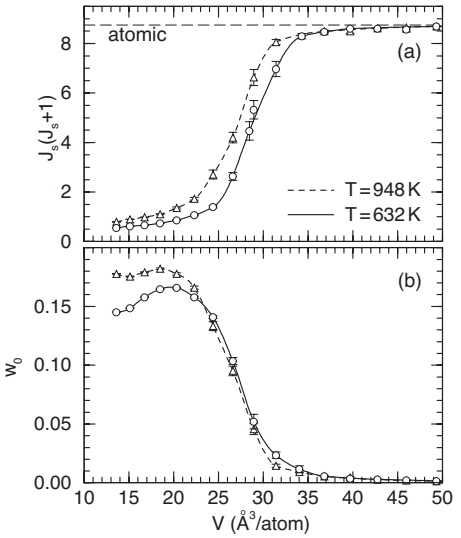


FIG. 3. Results for (a) the screened moment $J_s(J_s+1)=T\chi_J(\omega=0)$ and (b) the configuration weight $w_0$ for Ce at $T=948$ and 632 K as obtained with $L=80$ time slices.

$J_b(J_b+1)$ increases for $V<35$ Å$^3$/atom, as will be seen later. Since the $V(T_K)$ offset from 632 to 300 K is $\sim 1.3$ Å$^3$/atom,[25] we anticipate the 300 K $J_s(J_s+1)$ will be shifted to larger volume by $\sim 3$ Å$^3$/atom compared to our 632 K results. We find differences for $J_b(J_b+1)$ (not shown) to be smaller, with the analogous 948–632 K offset $\lesssim 1$ Å$^3$/atom in the vicinity of the transition and much smaller away from this regime.

### B. Charge susceptibility $\chi_c(\tau)$

The exact expression for the local charge susceptibility Eq. (4) may be written using the definitions Eqs. (9) and (10) as

$$\chi_c(\tau)=\sum_j N_j(\tau)+2\sum_{j\le j'} D_{jj'}(\tau)-n_f^2. \tag{14}$$

Following the language of Ref. 53 the local charge "fluctuations" are

$$\langle \delta\hat{n}_f^2\rangle \equiv \langle(\hat{n}_f-n_f)^2\rangle=\chi_c(\tau=0)=2d_f-n_f(n_f-1) \tag{15}$$

while the local *static* charge "susceptibility" is

$$\chi_c^{(1)}\equiv\chi_c(\omega=0)=\int_0^\beta d\tau\chi_c(\tau). \tag{16}$$

Note that $T\chi_c^{(1)}\le\langle\delta\hat{n}_f^2\rangle$ since $T\chi_c^{(1)}$ is the $\tau$ average of $\chi_c(\tau)$ which drops from its $\tau=0$, $\beta$ maxima of $\langle\delta\hat{n}_f^2\rangle$ to smaller values in the mid $\tau$ range, similar to Fig. 2 for the spin case. This upper bound for $T\chi_c^{(1)}$ is of interest since it helps to identify a large $\chi_c^{(1)}$, which signals the existence of prominent low-energy charge excitations as occurs, e.g., in the Yb valence transition.[53]

Clearly $\langle\delta\hat{n}_f^2\rangle$ and $T\chi_c^{(1)}$ are the charge susceptibility analogs of $J_b(J_b+1)$ and $J_s(J_s+1)$, respectively, for the spin case. Similarly, $\langle\delta\hat{n}_f^2\rangle$ and $T\chi_c^{(1)}$ must approach one another in the large-volume localized limit as $\hat{n}_f$ becomes an eigenoperator of the system with vanishing hybridization. However, in contrast to the spin case, $\langle\delta\hat{n}_f^2\rangle\to 0$ (and thus also $\chi_c^{(1)}\to 0$) in this limit for the trivalent rare earths since $n_f\to n$ and $d_f\to n(n-1)/2$, where $n$ is the nominal integer $4f$ occupation, e.g., $n=1$ for Ce.

The charge fluctuations $\langle\delta\hat{n}_f^2\rangle$ show negligible change for $V>22$ Å$^3$/atom on raising the temperature from 632 to 948 K for Ce in $L=80$ calculations, although are 10% larger by 14 Å$^3$/atom. The charge susceptibility $\chi_c^{(1)}$ is $\sim 60\%$ larger at the higher temperature, except at volumes near the transition, where the change is smaller.

## III. CONFIGURATION WEIGHTS

The probabilities or configuration weights $w_k$ of finding integer $k$ $f$-shell electrons on a given site are useful in discussing delocalization and are related to $\chi_c(\tau=0)=\langle\delta\hat{n}_f^2\rangle$ insofar as they may also be expressed as linear combinations of $n_f$ and $d_f$ near the localized limit. The $w_k$ are given by

$$w_k=Z_k/\sum_{k'} Z_{k'},$$

$$Z_k=\sum_{s_k}\langle ks_k|e^{-\beta(\hat{H}-\mu\hat{N})}|ks_k\rangle. \tag{17}$$

Here $\hat{H}$ is the Hamiltonian; $\hat{N}$, the total number operator for all types of electrons; $\mu$, the chemical potential; and $\{|ks_k\rangle\}$, a complete set of eigenstates of $\hat{n}_f$, $\hat{n}_f|ks_k\rangle=k|ks_k\rangle$, where all other quantum numbers besides $k$ are lumped into $s_k$. Evaluating the thermal expectations $\langle\cdots\rangle$ of 1, $\hat{n}_f$, and $\hat{n}_f(\hat{n}_f-1)/2$ using the same complete basis yields

$$1=\sum_k w_k,$$

$$n_f=\sum_k kw_k,$$

$$d_f=\sum_k k(k-1)w_k/2, \tag{18}$$

which shows the statistical nature of $n_f$ and $d_f$.

At sufficiently large volumes and low temperatures where only $w_k$ for $k=n$, $n\pm 1$ are non-negligible, these three $w_k$ may be expressed via Eq. (18) in terms of $n_f$ and $d_f$

$$w_{n-1}=d_f-d_f^{\min}(n_f)+(|n_f-n|-n_f+n)/2,$$

$$w_n=1-2[d_f-d_f^{\min}(n_f)]-|n_f-n|,$$

$$w_{n+1}=d_f-d_f^{\min}(n_f)+(|n_f-n|+n_f-n)/2. \tag{19}$$

Here it is convenient to use a function $d_f^{\min}(n_f)$ which is the minimum possible double occupation for an ensemble of sites whose average $f$-shell population is $n_f$. This is a piecewise linear function which assumes the values $k(k-1)/2$ at integer $k$ values of $n_f$ and may be expressed,

$$d_f^{\min}(n_f)=[n(n-1)+(2n-1)(n_f-n)+|n_f-n|]/2 \tag{20}$$

for the range $n-1\le n_f\le n+1$. Note that Eq. (19) gives the same results for Ce ($n=1$) as used before,[43] namely, $w_0=1$

$-n_f+d_f$, $w_1=n_f-2d_f$, and $w_2=d_f$. Even though spin orbit is now included while not in Ref. 43, we may still calculate the weights $w_k$ irrespective of how the $k$ electrons are distributed among the $j=5/2$ and 7/2 states, and this simpler diagnostic appears more than adequate for present discussion of delocalization.

Equation (19) appears intuitively to separate the effects of delocalization from those arising more simply out of changes in $n_f$ due to a possible $f$-shell electron reservoir. Should $n_f$ increase due to such a reservoir while the system is still in the strongly localized limit, where presumably $d_f=d_f^{\min}(n_f)$, then $w_{n-1}=0$, $w_n=1-n_f+n$, and $w_{n+1}=n_f-n$. This suggests $w_{n-1}$ is untainted by such reservoir effects for $n_f \geq n$ or more generally from Eq. (19)

$$d_f - d_f^{\min}(n_f) = \begin{cases} w_{n+1} & n-1 \leq n_f \leq n \\ w_{n-1} & n \leq n_f \leq n+1 \end{cases}, \tag{21}$$

which we argue in Sec. V is a useful diagnostic for delocalization. By contrast the local charge fluctuations

$$\langle \delta \hat{n}_f^2 \rangle = w_{n-1} + w_{n+1} - (n_f - n)^2 \tag{22}$$

appear to mix delocalization and reservoir effects and so are therefore less useful.

Figure 3(b) shows a test of the temperature sensitivities for the Ce configuration weight $w_0$ as calculated at 948 and 632 K with $L=80$ time slices. The offset for volumes $V>22$ Å$^3$/atom is less than 1 Å$^3$/atom, as generally found with other equal-time quantities. At smaller volumes both $w_0$ and $w_2$ increase with temperature, suggesting that higher temperature enhances delocalization in this volume range. This effect may be exaggerated in Fig. 3(b), however, as the 632 K $L=80$ result will be seen to be not yet fully converged with $L$ for $V<22$ Å$^3$/atom.

All $f$ configuration weights $w_0, w_1, \ldots, w_{14}$, may be obtained by using the higher multiple occupancies beyond $d_f$ in Eq. (18), which are trivially available in certain limits. In the extreme itinerant limit where hybridization has also dominated spin orbit, one might take $\langle \hat{n}_{\alpha_1} \hat{n}_{\alpha_2} \cdots \hat{n}_{\alpha_k} \rangle \sim (n_f/14)^k$, where $\alpha=j\nu$ and none of the $\alpha_i$ are equal. In this case it appears that the $w_{n\pm2}$ are reduced a factor of 2 or more over their adjacent $w_{n\pm1}$ and more distant $w_{n\pm k}$, by up to an order of magnitude over their adjacent weights closer to $n$. An overly localized limit, on the other hand, is provided by DMFT calculations using the atomiclike Hubbard I self-energy. Such results for Ce at 632 K give $w_1=1$ (or $w_1+w_2=1$ for $V<17.6$ Å$^3$/atom) with all other weights exponentially small. The validity of truncations such as Eq. (19) is justified by being close to a limit where the peripheral weights vanish, $w_{n\pm1} \to 0$ as we have at large volume, although Eq. (19) will eventually break down at sufficiently small volume.

## IV. COMPUTATIONAL DETAILS

The LDA+DMFT calculations reported in this paper have generally been carried out as in previous work on the compressed rare earths.[42–44] All calculations were performed for an assumed fcc structure and at a temperature of 632 K (4 mRy), with selected tests also at 948 K (6 mRy). The spin-orbit interaction was included in addition to the scalar part of the 4$f$ Coulomb interaction, i.e., the screened Slater integral $F^0 \equiv U_f$, however, not the higher Slater integrals ($F^k, k=2,4,6$) which describe the Hund's rules intra-atomic exchange. While this gives the wrong values for some 4$f$ moments in the localized limit, the volume dependence accompanying delocalization of these moments may still be reasonably captured as this appears to follow from fairly general behavior in the evolution of such quantities as the double occupancy. As in the earlier papers, the LDA contribution to the present work was provided by linear muffin-tin orbital calculations in the atomic-sphere approximation as described elsewhere.[4] The auxiliary Anderson impurity problem was solved using the Hirsch-Fye QMC algorithm,[54,55] with results obtained for $L=80$ and 112 time slices extrapolated to $L=\infty$ assuming a $1/L^2$ dependence. This was unnecessary for $\chi_J(\tau)$ where the two $L$ values gave essential agreement. The disposition of $U_f \hat{n}_f$ terms between the kinetic and interaction parts of the auxiliary impurity Hamiltonian in the Hirsch-Fye QMC, and the impact of this choice on Trotter corrections, is discussed in the Appendix.

The susceptibilities reported in this work were calculated within the QMC using Wick's theorem, e.g., Eq. (154) of Ref. 40. They were obtained from runs of ~350 000 and ~100 000 sweeps for $L=80$ and 112, respectively, using previously converged self-energies to get the input bath Green's functions. Error estimates were obtained from Eq. (5.3) of Ref. 56 in conjunction with an examination of the bin dependence of the data stored as a function of sweep.

## V. RESULTS

We now present results of the susceptibility and configuration weight calculations giving first comparisons between Ce, Pr, and Nd as a function of volume, then turning to insights provided by these results in regard to the experimentally observed transitions. Definitions of the quantities calculated have been presented in Secs. II and III. The volume range studied is from 10 to 50 Å$^3$/atom which may be compared to 300 K experimental volumes of 14.8, 14.1, and 14.2 Å$^3$/atom at a pressure of 100 GPa; and 34.4, 34.5, and 34.2 Å$^3$/atom at 0 GPa; for Ce,[10,57] Pr,[13,57] and Nd,[6,57] respectively.

Figure 4 shows results for $J(J+1)$ corresponding to the bare $J_b(J_b+1)=\chi_J(\tau=0)$ and screened $J_s(J_s+1)=T\chi_J(\omega=0)$ moments in Ce, Pr, and Nd, divided by the atomic-limiting values $J_a(J_a+1)=8.75$, 14, and 15.75, respectively, from Fig. 1. These are the "only spin-orbit" values of that figure, which give the correct $J(J+1)$ for Ce, however, are 30% and 36% smaller than the true Hund's rules values for Pr and Nd, respectively. It is particularly evident for the screened results that the changes are most abrupt and occur at the largest volumes for Ce, and then successively moderate and shift to smaller volume for Pr and then Nd, a pattern which will be seen throughout the present results. The bare moments increase with compression simply because the $n_f$ values increase.[58] Since a completely random population of the 4$f$ states would also have $\langle \hat{J}_z^2 \rangle$ and therefore $\langle \hat{\mathbf{J}}^2 \rangle$ increase with

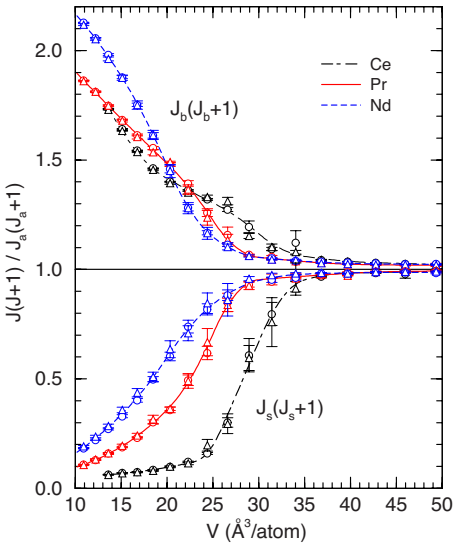


FIG. 4. (Color online) Bare $J_b(J_b+1)=\chi_J(\tau=0)$ and screened $J_s(J_s+1)=T\chi_J(\omega=0)$ moments for Ce, Pr, and Nd at 632 K, relative to the atomic-limiting values $J_a(J_a+1)$ of Fig. 1 for the only spin-orbit case. Smoothed curves are drawn through the points giving $L=80$ (circles) and 112 (triangles) results.

$n_f$, this does not imply the kind of coherent physical moment at the smallest volumes that one certainly has in the large-volume localized limit.

Figure 5 shows the local charge fluctuations $\langle \delta\hat{n}_f^2\rangle=\chi_c(\tau=0)$ and $T$ times the local static charge susceptibility $T\chi_c^{(1)}=T\chi_c(\omega=0)$, which are the charge analogs of the bare and

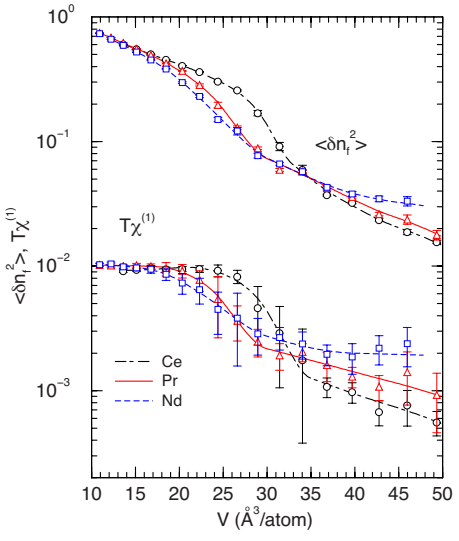


FIG. 5. (Color online) Local charge fluctuations $\langle \delta\hat{n}_f^2\rangle=\chi_c(\tau=0)$ and the static charge susceptibility $\chi_c^{(1)}=\chi_c(\omega=0)$, the latter multiplied by $T$, for Ce, Pr, and Nd at 632 K. Both show rapid increases under compression coincident with the changes observed in Fig. 4. $T\chi_c^{(1)}$ is everywhere more than an order of magnitude smaller than $\langle \delta\hat{n}_f^2\rangle$ reflecting the absence of low-energy charge fluctuations and the ratio $T\chi_c^{(1)}/\langle \delta\hat{n}_f^2\rangle$ becomes even smaller at small volumes reflecting screening of the charge fluctuations. All points are $1/L^2$ extrapolations to $L=\infty$, with smoothed curves drawn through them.

screened $J(J+1)$ of Fig. 4. Both quantities show rapid increases with compression in the same region as the changes seen in Fig. 4. Like the spin case these two quantities must also approach one another in the large-volume limit at low temperatures, although these limiting values are not finite but 0 for the charge case. This follows from $n_f\to n$ and $d_f\to n(n-1)/2$ in this limit, where $n=1$ (Ce), 2 (Pr), and 3 (Nd), and given that $\langle \delta\hat{n}_f^2\rangle=2d_f-n_f(n_f-1)$ from Eq. (15) and $\langle \delta\hat{n}_f^2\rangle\geq T\chi_c^{(1)}$ as discussed in Sec. II. The significance of the vanishing $4f$ charge fluctuations in the large-volume, low-temperature limit is disappearance of the Kondo resonance thus leaving a gapped $4f$ spectra overlapping the Fermi level.

Also interesting in Fig. 5 is how much smaller the local static charge susceptibility $\chi_c^{(1)}$ is compared to its limiting maximum $\langle \delta\hat{n}_f^2\rangle/T$, e.g., $T\chi_c^{(1)}/\langle \delta\hat{n}_f^2\rangle=0.017$, 0.031, and 0.033 at $V=15$, 28, and 41 Å$^3$/atom, respectively, for Ce, with similarly small values for Pr and Nd. In contrast this ratio is 0.25, 0.58, and 0.09 at the same volumes for the second to the last rare earth, Yb.[53] As pointed out in Ref. 53 the small ratios for Ce, Pr, and Nd constitute normal behavior where the large onsite Coulomb interaction suppresses low-energy charge excitations leading to a small local static susceptibility $\chi_c^{(1)}$. The oddball is Yb which has a valence transition from divalent ($f^{14}$) at large volume to trivalent ($f^{13}$) at small volume. The large Yb ratio 0.58 at 28 Å$^3$/atom is in the midst of the valence transition where the near degeneracy of $f^{13}$ and $f^{14}$ configurations leads to prominent low-energy charge excitations and a consequent large local static charge susceptibility. Finally, all four rare earths exhibit decreasing ratios $T\chi_c^{(1)}/\langle \delta\hat{n}_f^2\rangle$ for compression approaching the smallest volumes considered, which reflects screening of the charge fluctuations similar to screening of the moments as has been noted.[53]

The probability or configuration weight $w_k$ of finding integer $k$ $f$ electrons on a given site is of some interest in understanding the manner in which the rare earths evolve from localized to itinerant character under compression. As all sites are pinned at specific integer occupations $n$ in the large volume, localized limit at low temperatures, then for some range of smaller volumes away from this limit only $w_n$ and $w_{n\pm1}$ are non-negligible and may be determined from the average number of $4f$ electrons $n_f$ and their associated double occupation $d_f$ according to Eq. (19). Figure 6 shows $w_{n-1}$ and $w_{n+1}$ (the latter +0.1 for visual clarity) calculated in this manner for Ce, Pr, and Nd ($n=1$, 2, and 3, respectively). Equation (19) assumes $w_n=1-w_{n-1}-w_{n+1}$ so that the limit $w_n=1$ and $w_{k\neq n}=0$ is evidently being approached at large volumes.

As volume is reduced away from the localized limit, two things happen. First, for purely one-electron reasons, the $6s$ and $6p$ bands rise relative to the $4f$ levels, causing an increase in $n_f$ (Ref. 58) and thus a shift in weight from $w_n$ to $w_{n+1}$. Second, as hybridization grows, the $4f$ electrons begin to hop to $f$ states on neighboring sites or into and out of valence levels, causing *both* $w_{n\pm1}$ to grow at the expense of $w_n$. Only $w_{n-1}$ is a true measure of the second, delocalization effect uncomplicated by the consequences of increasing $n_f$.[59] Or more generally, this diagnostic for delocalization is given by Eq. (21) which is $w_{n-1}$ for $n_f\geq n$ and $w_{n+1}$ for $n_f\leq n$.

Figure 6 shows clear evidence of both the rising $6s$ and $6p$ bands and delocalization. Note first the onset of delocaliza-

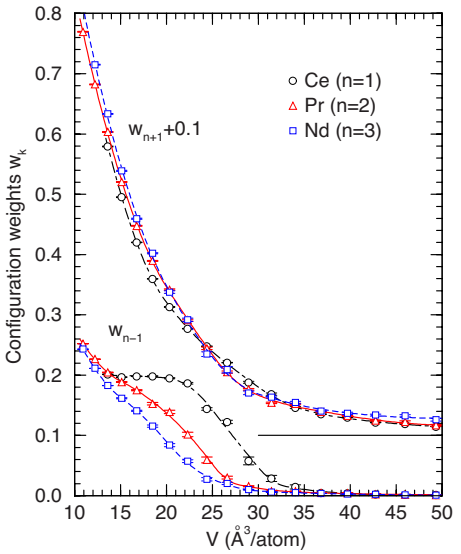


FIG. 6. (Color online) Configuration weights $w_{n-1}$ and $w_{n+1}$ (latter +0.1) for Ce ($n=1$), Pr ($n=2$), and Nd ($n=3$). The former is a measure of delocalization $w_{n-1}=d_f-d_f^{\min}(n_f)$ since $n\lesssim n_f<n+1$ everywhere and shows a dramatic rise with compression for Ce, structure which successively softens and shifts to smaller volumes in moving to Pr and then Nd. The weights $w_{n+1}$ are complicated by the general increase in $n_f$ with compression due to the rising 6$s$ and 6$p$ bands. All points are $1/L^2$ extrapolations to $L=\infty$, with smoothed curves drawn through them.

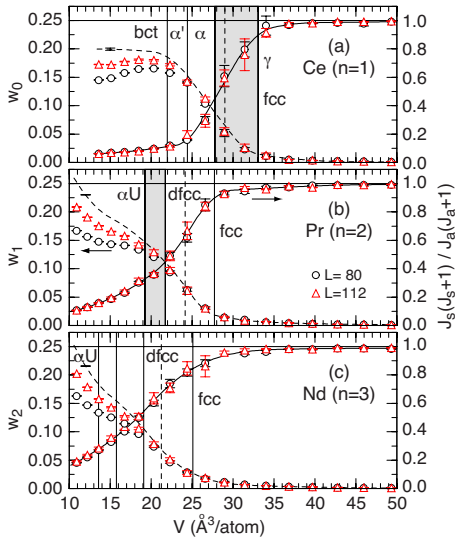


FIG. 7. (Color online) Screened moments $J_s(J_s+1)$ (solid curves) and configuration weights $w_{n-1}$ (dashed curves) for (a) Ce, (b) Pr, and (c) Nd. All calculations are for an assumed fcc structure at 632 K, however, are compared to the observed 300 K phases demarcated by the vertical lines, with shading for Ce and Pr indicating significant two-phase regions. Theoretical temperature sensitivities are discussed in the text. The moments appear divided by their atomic-limiting values $J_a(J_a+1)$ of Fig. 1 for the only spin-orbit case. The smoothed curves are drawn through the combined $L=80$ (circles) and 112 (triangles) points for the moments, and extrapolated to $L\to\infty$ for the $w_{n-1}$. The vertical dashed lines show the volumes where the Kondo temperature is 632 K.

tion as $w_{n-1}$ increases with compression and how much more abrupt this behavior is compared to the smoother $w_{n+1}$ curves which reflect also the effects of increasing $n_f$. These onsets occur near the equilibrium volume of Ce ($V_0$ =34.37 Å$^3$/atom) but at somewhat smaller volumes than the corresponding $V_0$ of Pr (34.54) and Nd (34.17). At the largest volumes ($V>42$ Å$^3$/atom), $w_{n+1}$ is an order of magnitude larger than $w_{n-1}\leq 0.003$ for all three rare earths, suggesting the behavior there is predominantly the increase in $n_f$ due to the rising 6$s$ and 6$p$ bands. Since the Fermi level in this regime lies in between and does not overlap either of the two Hubbard bands, this suggests that the large-volume shift in weight $w_n\to w_{n+1}$ is not mixed valence in the sense of the Fermi level moving into the upper Hubbard band but rather that the rising 6$s$ and 6$p$ bands transfer electrons into the 4$f$ quasiparticle peak, which is nonetheless still quite small in this region.[60]

There have been experimental determinations of the Ce configuration weights $w_{0,1,2}$ using Anderson impurity model analyses of photoemission[27] and resonant inelastic x-ray scattering[22] data, and a number of LDA+DMFT calculations[41–44,46] of these quantities or related $n_f=1-w_0+w_2$. All are consistent with $w_1\to 1$ and $w_{k\neq 1}\to 0$ in the large-volume limit. There is an asymmetry between $f^1$-$f^0$ and $f^1$-$f^2$ mixing in solutions of the Anderson impurity model which tends to lead to the predominant transfer $w_1\to w_0$ with growing hybridization, and thus a decrease in $n_f$ across the $\gamma$ to $\alpha$ collapse and $w_0>w_2$ in the $\alpha$ phase.[28] This behavior is seen in the analyses of both experimental papers.[22,27] The present and our earlier work[42–44] concur with the predominant transfer $w_1\to w_0$ across the collapse, however, has everywhere a larger $w_2$ than these analyses, quite possibly reflecting the impact on $n_f$ of the rising 6$s$ and 6$p$ bands which may not be well treated in the impurity model simulations. Thus we see a nonmonotonic dip in $n_f$ across the collapse but generally $n_f>1$ and $w_0<w_2$.[58]

We turn now to possible insights provided by the present results into the experimentally observed 300 K volume collapse transitions (shaded regions) and phase structure (demarcated by vertical solid lines) as shown in Fig. 7 for Ce,[8–10] Pr,[12–15] and Nd.[5,6] At large volume only the fcc phase is labeled, which is the end of the localized, trivalent rare-earth series,[1] with all three rare earths found in the preceding, double-hexagonal-close-packed phase at ambient conditions. The two most dramatic theoretical diagnostics are shown for comparison, $J_s(J_s+1)$ and $w_{n-1}$, and while they were calculated everywhere assuming an fcc structure, it is hoped nonetheless that their volume dependence is sufficiently insensitive to structure so as to still provide useful insights. This is not an issue for Ce where both $\alpha$ and $\gamma$ phases bounding the volume collapse are fcc. While the theory results are for 632 K, temperature sensitivities examined in Secs. II and III for Ce suggest the predominant difference on reducing the temperature to 300 K would be a ~3 Å$^3$/atom shift of the $J_s(J_s+1)$ curves to larger volume and perhaps half that shift for the $w_{n-1}$ curves.

LDA+DMFT calculations[41–46] have consistently supported the KVC scenario[25–28] for Ce. They show, e.g., a rapid build up of the Kondo resonance for volume reduced across the $\gamma$-$\alpha$ two-phase region, which is taken as a signature of

the onset of screening. The present results now directly report the screened moment and indeed one sees a large reduction in $J_s(J_s+1)$ from the $\gamma$ to the $\alpha$ side of the collapse. Moreover, if the Kondo temperature $T_K$ is defined by the condition $T\chi_J(\omega=0)/\chi_J(\tau=0)=0.5$, then $T_K=632$ K at the volume $V=29.0$ Å$^3$/atom (vertical dashed line) for the isothermal results in Fig. 7(a). This value is consistent with the combined experimental results of Refs. 22 and 27, except for the middle 10 kbar point of the former which appears out of place given the roughly exponential behavior expected for $T_K(V)$.[25]

The competing MT scenario for the Ce volume collapse relies on $4f$ electron delocalization as the underlying driving mechanism.[23,24] If Eq. (21) is accepted as one suitable diagnostic, then $w_0$ in Fig. 7(a) suggests that the collapse also coincides with delocalization, a point that has been made previously.[42,43] To be careful, note that Eq. (19) for the $w_k$ does break down when configurations $f^k$ for $|k-n|\geq 2$ become important as the itinerant limit is approached, as discussed in Sec. III. It would seem from the present and earlier LDA+DMFT calculations that the following are all different facets of the same continuous and extended evolution with compression of a nominally $f^n$ trivalent rare earth: (1) transfer of $4f$ spectral weight from Hubbard side bands to a Fermi-level structure, (2) screening of the $4f$ moments, (3) growth of $4f$ charge fluctuations, and (4) dispersal of configuration weight away from $w_n=1$ to neighboring and then more distant configurations. Some of these facets look more Kondo like and some seem more consistent with intuitive ideas of delocalization.

There is striking similarity between the theoretical diagnostics for Ce and those for Pr and Nd in Fig. 7, although the screening and delocalization effects shift to smaller volume and become more gradual for Pr, and then more so for Nd. The stability fields of the distorted fcc (dfcc) structures in both Pr and Nd appear analogous to the $\alpha$-$\gamma$ two-phase region in Ce, according to progression of the two theoretical diagnostics. Only on further compression is there a volume collapse in Pr from dfcc to $\alpha$-$U$ while Nd passes through two additional phases before reaching the same $\alpha$-$U$ structure, absent any large-volume changes. It is conceivable that this progression in collapse size and location follows simply from the shift to smaller volumes and moderation in the correlation contributions which must then compete with the ever bigger underlying benign part of the equation of state. While there are suggestions of a Van der Waals loop in the LDA+DMFT free energy corresponding to the isostructural fcc Ce collapse,[42–44,46] one must worry about the need to include the proper Hund's rules exchange for multi-$f$ electron Pr and Nd, as well as performing the calculations for all of the observed structures, e.g., $\alpha$-$U$. Moreover, the Ce collapse has a critical temperature of only 480 K (Ref. 61) while for Pr, the dfcc phase is absent above about 700 K with yet a new Pr-VI phase intermediate between the $\alpha$-$U$ and fcc phases.[14] These temperature sensitivities are also a reminder of the need to include lattice vibrational contributions, which may themselves further modify the nature of the collapse transitions.[61,62]

## VI. SUMMARY

We have reported LDA+DMFT calculations as a function of volume at 632 K, for the $4f$ spin and charge susceptibilities, and the probabilities of finding $4f^{n\pm1}$ configurations in the nominally $4f^n$ trivalent rare earths Ce ($n=1$), Pr ($n=2$), and Nd ($n=3$). We find these metals to remain localized at pressures up through the fcc ($\gamma$-Ce) phases, the last structure of the initial close-packed series,[1] as indicated by sharp $4f^n$ populations, unscreened moments with atomic-limiting values, and small charge fluctuations indicating little $4f$ state density overlapping the Fermi level. On subsequent compression there is rapid and dramatic screening of the moments and concurrent increase in charge fluctuations and the static charge susceptibility. These changes also coincide with rapid growth in the $4f^{n-1}$ configuration weights, which we argue offer a truer measure of delocalization than do the $4f^{n+1}$ weights which are complicated by the overall increase in the number of $4f$ electrons due to the rising $6s$ and $6p$ bands. Combined with earlier LDA+DMFT results, this work suggests a continuous and extended evolution with compression of a nominally $4f^n$ trivalent rare earth in which there is (1) transfer of $4f$ spectral weight from Hubbard side bands to the vicinity of the Fermi level, (2) screening of the $4f$ moments, (3) growth of $4f$ charge fluctuations, and (4) dispersal of configuration weight away from $4f^n$ to adjacent and then more distant configurations $4f^k$. The static charge susceptibility $\chi_c^{(1)}$ mirrors the volume dependence of the charge fluctuations $\langle \delta\hat{n}_f^2 \rangle$ and further indicates screening of these fluctuations at small volume, and suppression of low-energy charge fluctuations by the Coulomb interaction at all volumes.[53]

This work suggests that a proper understanding of the volume collapse transitions in the compressed trivalent rare earths will require their analysis in the context of diagnostics for the underlying and robust evolution associated with $4f$-electron delocalization. Much effort remains here, including a clearer understanding of the approach to the itinerant limit in terms of all of the configuration weights as well as the vanishing Hubbard spectral features, and an examination of the relation between electron delocalization and screening of the moments. As to the thermodynamics, LDA+DMFT calculations do hint at a Van der Waals loop in the Ce free energy at about the right place,[42–44,46] however, the full story for Pr and Nd may await inclusion of the Hund's rules exchange for these multi-$f$ electron cases and assumption of the correct structures for all phases (e.g., $\alpha$-$U$). The Ce case also raises the prospect of the need for lattice vibrational contributions in all cases.[61,62]

## ACKNOWLEDGMENTS

Work by A.K.M. was performed under the auspices of the U.S. Department of Energy by Lawrence Livermore National Laboratory under Contract No. DE-AC52-07NA27344. Work by M.J. and R.T.S. was supported by the SciDAC program under Grant No. DOE-DE-FC0206ER25793 and that by R.T.S. also by the DOE SSAAP program. This work has also benefited from an alliance with members of the DOE/

BES funded Computational Materials Science Network Cooperative Research Team on "Predictive Capability for Strongly Correlated Systems." A.K.M. is grateful for conversations with K. Held, J. Kuneš, W. E. Pickett, and E. R. Ylvisaker.

## APPENDIX: TROTTER CORRECTIONS AND THE BATH GREEN'S FUNCTION

One issue related to application of Hirsch-Fye[54] QMC to the rare-earth series deserves attention. It illustrates remark (iii) on page 910 of Ref. 38 for the present case, where we suggest a related but slightly different choice for the modified impurity problem. To prepare for the Hubbard-Stratonovich transformation, one rewrites the interaction part $\hat{I}$ of the auxiliary impurity Hamiltonian

$$U_f \sum_{\alpha<\alpha'} \hat{n}_\alpha \hat{n}_{\alpha'} = U_f \sum_{\alpha<\alpha'} \left[ \hat{n}_\alpha \hat{n}_{\alpha'} - \frac{1}{2}(\hat{n}_\alpha + \hat{n}_{\alpha'}) \right] + \frac{13}{2} U_f \hat{n}_f, \tag{A1}$$

where $\alpha$ labels the $14f$ states. A strict generalization of the Hirsch-Fye treatment would be to remove the $U_f \hat{n}_f$ term from the right side of in Eq. (A1) and add it to the one-body or kinetic-energy part $\hat{K}$ of the Hamiltonian, with the consequent changes in unperturbed or bath Green's function $\mathcal{G}(\tau)$ and also the Trotter breakup. However, for $U_f = 6$ eV and $T = 600$ K, this would lead to an $f$ bath Green's function, absent hybridization and spin orbit for simplicity, of

$$\mathcal{G}_f(\tau) = -\frac{1}{14} \sum_\alpha \mathrm{Tr}[\hat{\rho} f_\alpha(\tau) f_\alpha^\dagger(0)]/\mathrm{Tr}[\hat{\rho}] \sim \frac{-e^{-\tau(\varepsilon_f + 6.5U_f - \mu)}}{e^{-\beta(\varepsilon_f + 6.5U_f - \mu)} + 1}$$
$$\sim -10^{-300\tau/\beta}. \tag{A2}$$

Here $\hat{\rho} = \exp[-\beta(\hat{K} - \mu\hat{N})]$, $\mu$ is the chemical potential, $\hat{N}$ the total electron number operator, $0 < \tau < \beta$, and we take a Ce-like site energy $\varepsilon_f - \mu \sim -U_f/2$. Such a function may get into a region of underflow errors at large $\tau$ in numerical computation. Note this problem arises here in the seven-band case only because the $U_f \hat{n}_f$ term in question is 13 times larger than in the familiar one-band case. For this reason we left the $U_f \hat{n}_f$ term alone in previous work on the early rare earths,[42–44] and took the kinetic and interaction parts of the auxiliary impurity Hamiltonian to be

$$\hat{K} = \varepsilon_f \hat{n}_f + \sum_{\lambda,\lambda'} c_\lambda^\dagger \Delta t_{\lambda\lambda'} c_{\lambda'}, \tag{A3}$$

$$\hat{I} = U_f \sum_{\alpha<\alpha'} \left[ \hat{n}_\alpha \hat{n}_{\alpha'} - \frac{1}{2}(\hat{n}_\alpha + \hat{n}_{\alpha'}) \right] + \frac{13}{2} U_f \hat{n}_f, \tag{A4}$$

where $\lambda$ ranges over both $f$ and the additional bath degrees of freedom, and $\Delta t$ covers the rest of the one-body terms. Keeping the $U_f \hat{n}_f$ term in $\hat{I}$ can be handled with a minor modification of the Hirsch-Fye technique.

Since $\varepsilon_f - \mu$ itself varies from about $-0.5U_f$ for Ce to about $-6.5U_f$ for Lu, the choice Eq. (A3) then leads to similar problems for the bath Green's function of the late rare earths. A more consistent treatment for the series as a whole would be to use one of the Hubbard bands as the effective $f$ site energy in the bath Green's function, and we use the approximate position of the lower Hubbard band, $\varepsilon_{\mathrm{LH}} = \varepsilon_f + (n-1)U_f$, with the integer $n$ being the nominal $f$ occupation. Thus we take

$$\hat{K} = [\varepsilon_f + (n-1)U_f]\hat{n}_f + \sum_{\lambda,\lambda'} c_\lambda^\dagger \Delta t_{\lambda\lambda'} c_{\lambda'}, \tag{A5}$$

$$\hat{I} = U_f \sum_{\alpha<\alpha'} \left[ \hat{n}_\alpha \hat{n}_{\alpha'} - \frac{1}{2}(\hat{n}_\alpha + \hat{n}_{\alpha'}) \right] + \left( \frac{15}{2} - n \right) U_f \hat{n}_f, \tag{A6}$$

which was successfully used in Hirsch-Fye calculations for the second to last rare earth, Yb ($n=13$) (Ref. 53) while for Ce ($n=1$), Eqs. (A5) and (A6) are identical to Eqs. (A3) and (A4).

We note here that even for the light rare earths such as Pr ($n=2$) and Nd ($n=3$) that Eqs. (A5) and (A6) serve to accelerate convergence of the susceptibilities with increasing $L$ relative to Eqs. (A3) and (A4). This is seen for Nd in Fig. 8, where the instantaneous spin $\chi_J(\tau=0) = J_b(J_b+1)$ and charge $\chi_c(\tau=0) = \langle \delta\hat{n}_f^2 \rangle$ susceptibilities are shown as functions of volume. Results using $\varepsilon_f$ [Eqs. (A3) and (A4), circles, up triangles] and $\varepsilon_{\mathrm{LH}}$ [Eqs. (A5) and (A6), squares, down triangles] as effective $f$ site energies are given for $L=80$ and 112 time slices. The former points are quite different indicating significant Trotter corrections while the latter are essentially on top of one another except for the charge case at the smallest volumes. It is reassuring that $L^{-2}$ extrapolations to

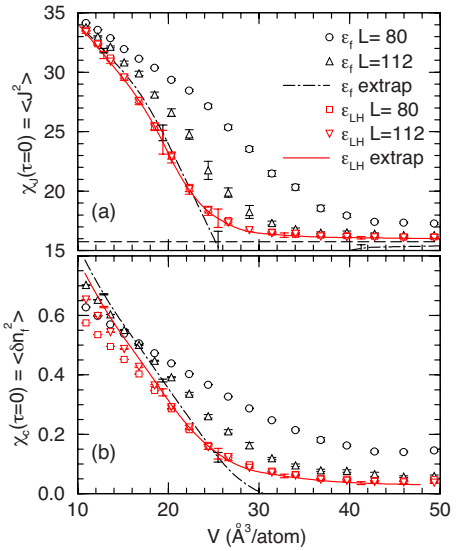


FIG. 8. (Color online) Trotter corrections in (a) $\chi_J(\tau=0) = \langle \hat{\mathbf{J}}^2 \rangle$ and (b) $\chi_c(\tau=0) = \langle \delta\hat{n}_f^2 \rangle$ for Nd as a function of volume. Results for $L=80$ and 112 time slices are shown, using the $\varepsilon_f$ (circles, up triangles) and $\varepsilon_{\mathrm{LH}}$ (squares, down triangles) effective $f$ site energies in the QMC. The lines show $L^{-2}$ extrapolation to $L=\infty$. It is evident that the Trotter corrections are considerably smaller using the $\varepsilon_{\mathrm{LH}}$ choice Eqs. (A5) and (A6). The horizontal dashed line in (a) is the atomic-limiting value.

$L=\infty$ (lines) for the $\varepsilon_f$ and $\varepsilon_{\mathrm{LH}}$ cases are fairly close at smaller volumes. On the other hand, extrapolation of the $\varepsilon_f$ results yields an unphysical negative $\chi_c(\tau=0)$ at large volumes (not shown) indicating non-$L^{-2}$ behavior and the need for larger $L$. By contrast the $\varepsilon_{\mathrm{LH}}$ results are already converged by $L=80$ for both spin and charge cases at large volume. While we believe both approaches will give the same results for Ce, Pr, and Nd in the limit $L\to\infty$, it is clear that Eqs. (A5) and (A6) converge faster with $L$, and all results in the present paper have been obtained in this manner.


[1] J. C. Duthie and D. G. Pettifor, Phys. Rev. Lett. **38**, 564 (1977).
[2] U. Benedict, J. Alloys Compd. **193**, 88 (1993).
[3] W. B. Holzapfel, J. Alloys Compd. **223**, 170 (1995).
[4] A. K. McMahan, C. Huscroft, R. T. Scalettar, and E. L. Pollock, J. Comput.-Aided Mater. Des. **5**, 131 (1998).
[5] J. Akella, S. T. Weir, Y. K. Vohra, H. Prokop, S. A. Catledge, and G. N. Chesntnut, J. Phys.: Condens. Matter **11**, 6515 (1999).
[6] G. N. Chesnut and Y. K. Vohra, Phys. Rev. B **61**, R3768 (2000).
[7] D. G. Koskimaki and K. A. Gschneidner, Jr., in *Handbook on the Physics and Chemistry of Rare Earths*, edited by K. A. Gschneidner, Jr. and L. R. Eyring (North-Holland, Amsterdam, 1978), p. 337.
[8] J. S. Olsen, L. Gerward, U. Benedict, and J. P. Itié, Physica B & C **133**, 129 (1985).
[9] M. I. McMahon and R. J. Nelmes, Phys. Rev. Lett. **78**, 3884 (1997).
[10] Y. K. Vohra, S. L. Beaver, J. Akella, C. A. Ruddle, and S. T. Weir, J. Appl. Phys. **85**, 2451 (1999).
[11] H. K. Mao, R. M. Hazen, P. M. Bell, and J. Wittig, J. Appl. Phys. **52**, 4572 (1981); G. S. Smith and J. Akella, *ibid.* **53**, 9212 (1982); W. A. Grosshans and W. B. Holzapfel, J. Phys. (Paris) **45**, C8 (1984).
[12] Y. C. Zhao, F. Porsch, and W. B. Holzapfel, Phys. Rev. B **52**, 134 (1995).
[13] G. N. Chesnut and Y. K. Vohra, Phys. Rev. B **62**, 2965 (2000).
[14] B. J. Baer, H. Cynn, V. Iota, C.-S. Yoo, and G. Shen, Phys. Rev. B **67**, 134115 (2003).
[15] N. C. Cunningham, N. Velisavljevic, and Y. K. Vohra, Phys. Rev. B **71**, 012108 (2005).
[16] H. Hua, Y. K. Vohra, J. Akella, S. T. Weir, R. Ahuja, and B. Johansson, Rev. High Pressure Sci. Technol. **7**, 233 (1998).
[17] R. Patterson, C. K. Saw, and J. Akella, J. Appl. Phys. **95**, 5443 (2004).
[18] K. A. McEwen, *Handbook on the Physics and Chemistry of Rare Earths* (Ref. 7), Vol. 1, p. 411, see Table 6.1.
[19] J. W. Ward, P. D. Kleinschmidt, and D. E. Peterson, in *Handbook on the Physics and Chemistry of the Actinides*, edited by A. J. Freeman and C. Keller (North-Holland, Amsterdam, 1986), Vol. 4, p. 309.
[20] A. P. Murani, S. J. Levett, and J. W. Taylor, Phys. Rev. Lett. **95**, 256403 (2005).
[21] B. R. Maddox, A. Lazicki, C. S. Yoo, V. Iota, M. Chen, A. K. McMahan, M. Y. Hu, P. Chow, R. T. Scalettar, and W. E. Pickett, Phys. Rev. Lett. **96**, 215701 (2006).
[22] J.-P. Rueff, J.-P. Itié, M. Taguchi, C. F. Hague, J.-M. Mariot, R. Delaunay, J.-P. Kappler, and N. Jaouen, Phys. Rev. Lett. **96**, 237403 (2006).
[23] B. Johansson, Philos. Mag. **30**, 469 (1974).
[24] B. Johansson, Phys. Rev. B **11**, 2740 (1975).
[25] J. W. Allen and R. M. Martin, Phys. Rev. Lett. **49**, 1106 (1982).
[26] M. Lavagna, C. Lacroix, and M. Cyrot, Phys. Lett. **90A**, 210 (1982).
[27] L. Z. Liu, J. W. Allen, O. Gunnarsson, N. E. Christensen, and O. K. Andersen, Phys. Rev. B **45**, 8934 (1992).
[28] J. W. Allen and L. Z. Liu, Phys. Rev. B **46**, 5047 (1992).
[29] O. Eriksson, M. S. S. Brooks, and B. Johansson, Phys. Rev. B **41**, 7311 (1990).
[30] I. S. Sandalov, O. Hjortstam, B. Johansson, and O. Eriksson, Phys. Rev. B **51**, 13987 (1995).
[31] A. B. Shick, W. E. Pickett, and A. I. Liechtenstein, J. Electron Spectrosc. Relat. Phenom. **114–116**, 753 (2001).
[32] P. Söderlind, Phys. Rev. B **65**, 115105 (2002).
[33] Z. Szotek, W. M. Temmerman, and H. Winter, Phys. Rev. Lett. **72**, 1244 (1994).
[34] A. Svane, Phys. Rev. Lett. **72**, 1248 (1994); Phys. Rev. B **53**, 4275 (1996).
[35] A. Svane, J. Trygg, B. Johansson, and O. Eriksson, Phys. Rev. B **56**, 7143 (1997).
[36] O. Gunnarsson and K. Schönhammer, Phys. Rev. Lett. **50**, 604 (1983); Phys. Rev. B **28**, 4315 (1983); **31**, 4815 (1985).
[37] K. Held, I. A. Nekrasov, G. Keller, V. Eyert, N. Blumer, A. K. McMahan, R. T. Scalettar, T. Pruschke, V. I. Anisimov, and D. Vollhardt, Phys. Status Solidi B **243**, 2599 (2006).
[38] G. Kotliar, S. Y. Savrasov, K. Haule, V. S. Oudovenko, O. Parcollet, and C. A. Marianetti, Rev. Mod. Phys. **78**, 865 (2006).
[39] D. Vollhardt, in *Correlated Electron Systems*, edited by V. J. Emery (World Scientific, Singapore, 1993), Vol. 57; Th. Pruschke, M. Jarrell, and J. K. Freericks, Adv. Phys. **44**, 187 (1995).
[40] A. Georges, G. Kotliar, W. Krauth, and M. Rozenberg, Rev. Mod. Phys. **68**, 13 (1996).
[41] M. B. Zölfl, I. A. Nekrasov, Th. Pruschke, V. I. Anisimov, and J. Keller, Phys. Rev. Lett. **87**, 276403 (2001).
[42] K. Held, A. K. McMahan, and R. T. Scalettar, Phys. Rev. Lett. **87**, 276404 (2001).
[43] A. K. McMahan, K. Held, and R. T. Scalettar, Phys. Rev. B **67**, 075108 (2003).
[44] A. K. McMahan, Phys. Rev. B **72**, 115125 (2005).
[45] K. Haule, V. Oudovenko, S. Y. Savrasov, and G. Kotliar, Phys. Rev. Lett. **94**, 036401 (2005).
[46] B. Amadon, S. Biermann, A. Georges, and F. Aryasetiawan, Phys. Rev. Lett. **96**, 066402 (2006).
[47] K. Held and R. Bulla, Eur. Phys. J. B **17**, 7 (2000).
[48] P. van Dongen, K. Majumdar, C. Huscroft, and F.-C. Zhang, Phys. Rev. B **64**, 195123 (2001).
[49] L. de' Medici, A. Georges, G. Kotliar, and S. Biermann, Phys. Rev. Lett. **95**, 066402 (2005).
[50] A. Koga, N. Kawakami, T. M. Rice, and M. Sigrist, Phys. Rev. B **72**, 045128 (2005).
[51] B. Amadon, F. Jollet, and M. Torrent, Phys. Rev. B **77**, 155104 (2008).

[52] F. Herman and S. Skillman, *Atomic Structure Calculations* (Prentice-Hall, Englewood Cliffs, NJ, 1963).
[53] E. R. Ylvisaker, J. Kuneš, A. K. McMahan, and W. E. Pickett, Phys. Rev. Lett. **102**, 246401 (2009).
[54] J. E. Hirsch and R. M. Fye, Phys. Rev. Lett. **56**, 2521 (1986).
[55] See Ref. 40 and M. Jarrell, in *Numerical Methods for Lattice Quantum Many-Body Problems*, edited by D. Scalapino (Addison-Wesley, Reading, MA, 1997) for one-band DMFT (QMC).
[56] M. Jarrell and J. E. Gubernatis, Phys. Rep. **269**, 133 (1996).
[57] D. A. Young, *Phase Diagrams of the Elements* (University of California, Berkeley, 1991).
[58] Fig. 2 in Ref. 44 shows $n_f \gtrsim n$ for Ce ($n=1$), Pr (2), and Nd (3), with $n_f$ monotonically increasing under compression except for Ce in the range $24 \leq V \leq 29$ Å$^3$/atom.
[59] For a single-band Hubbard model at fixed filling $n=1$, the weights $w_{n-1}=w_{n+1}$ contain identical information concerning possible localization transitions. One can partially restore this symmetry even in the present multiband case, when the filling drifts away from integer values, by subtracting off the excess density. In particular, the identities in Eq. (18) yield $w_{n+1} - [n_f - n] = w_{n+1} - [(n-1)w_{n-1} + nw_n + (n+1)w_{n+1}] = w_{n+1} - [-w_{n-1} + w_{n+1}] = w_{n-1}$. Note, however, that the asymmetry between $f^1$-$f^0$ and $f^2$-$f^1$ mixing described in Ref. 28 suggests this attempt to make the two weights equivalent should not be pushed too strongly.
[60] Additional evidence that the increase in $n_f$ over $n$ at large volumes involves the quasiparticle peak comes from DMFT calculations with the Hubbard I self-energy which are incapable of generating the quasiparticle peak. In this approximation $n_f$ is found to remain pinned to $n$ until quite small volumes, e.g., for all $V > 17.6$ Å$^3$/atom in Ce.
[61] M. J. Lipp, D. Jackson, H. Cynn, C. Aracne, W. J. Evans, and A. K. McMahan, Phys. Rev. Lett. **101**, 165703 (2008).
[62] I.-K. Jeong, T. W. Darling, M. J. Graf, Th. Proffen, R. H. Heffner, Yongjae Lee, T. Vogt, and J. D. Jorgensen, Phys. Rev. Lett. **92**, 105702 (2004).